Do mantle plumes preserve the heterogeneous structure of their deep-mantle source?

T.D. Jones [a],[*], D.R. Davies [a], I.H. Campbell [a], C.R. Wilson [b], S.C. Kramer [c]

[a] Research School of Earth Sciences, The Australian National University, Canberra, Australia
[b] Lamont-Doherty Earth Observatory, Columbia University, New York, USA
[c] Department of Earth Science and Engineering, Imperial College, London, UK

A B S T R A C T

It has been proposed that the spatial variations recorded in the geochemistry of hotspot lavas, such as the bilateral asymmetry recorded at Hawaii, can be directly mapped as the heterogeneous structure and composition of their deep-mantle source. This would imply that source-region heterogeneities are transported into, and preserved within, a plume conduit, as the plume rises from the deep-mantle to Earth's surface. Previous laboratory and numerical studies, which neglect density and rheological variations between different chemical components, support this view. However, in this paper, we demonstrate that this interpretation cannot be extended to distinct chemical domains that differ from surrounding mantle in their density and viscosity. By numerically simulating thermo-chemical mantle plumes across a broad parameter space, in 2-D and 3-D, we identify two conduit structures: (i) bilaterally asymmetric conduits, which occur exclusively for cases where the chemical effect on buoyancy is negligible, in which the spatial distribution of deep-mantle heterogeneities is preserved during plume ascent; and (ii) concentric conduits, which occur for all other cases, with dense material preferentially sampled within the conduit's centre. In the latter regime, the spatial distribution of geochemical domains in the lowermost mantle is not preserved during plume ascent. Our results imply that the heterogeneous structure and composition of Earth's lowermost mantle can only be mapped from geochemical observations at Earth's surface if chemical heterogeneity is a passive component of lowermost mantle dynamics (i.e. its effect on density is outweighed by, or is secondary to, the effect of temperature). The implications of our results for: (i) why oceanic crust should be the prevalent component of ocean island basalts; and (ii) how we interpret the geochemical evolution of Earth's deep-mantle are also discussed.

© 2015 Elsevier B.V. All rights reserved.

1. Introduction

Mantle plumes are buoyant upwellings that bring hot material from Earth's deep-mantle to its surface, generating large igneous provinces (LIPs) and volcanic island chains, such as the Siberian Traps and the Hawaiian–Emperor chain, respectively (e.g. Morgan, 1972; Richards et al., 1989; Campbell and Griffiths, 1990; Griffiths and Campbell, 1991; Davies, 1992; Farnetani and Richards, 1994, 1995; Leitch and Davies, 2001; Davies and Davies, 2009; Davies et al., 2015b, 2015c). Although mantle plumes represent the only source of volcanism on Earth that directly samples the lowermost mantle, it remains unclear how their variable geochemical expression at Earth's surface (i.e. the geochemical variations recorded in volcanic hotspot lavas) relates to the heterogeneous structure of their deep-mantle source (e.g. Dupré and Allègre, 1983; Allègre et al., 1996; Tackley, 1998; Hofmann, 2003). For example, the most recent 2–3 Myr of volcanism along the Hawaiian–Emperor chain is defined by two parallel volcanic island tracks, the Loa- and Kea-tracks (Jackson et al., 1975), which exhibit distinct geochemical signatures (e.g. Tatsumoto, 1978; Abouchami et al., 2005). Southern Loa-track volcanoes are generally less depleted, displaying systematically higher $^{208}Pb/^{204}Pb$ at a given $^{206}Pb/^{204}Pb$, as well as higher $^{87}Sr/^{86}Sr$ and lower $^{143}Nd/^{144}Nd$, when compared to the Northern Kea-track volcanoes (e.g. Abouchami et al., 2005). While several hypotheses have been proposed to explain such systematic variations (e.g. Bianco et al., 2008, 2011; Ballmer et al., 2011, 2013, 2015), the most prominent attributes them to internal zonation within the underlying mantle plume conduit, which may relate directly to large-scale geochemical domains in the lowermost mantle (e.g. Abouchami et al., 2005; Weis et al., 2011;
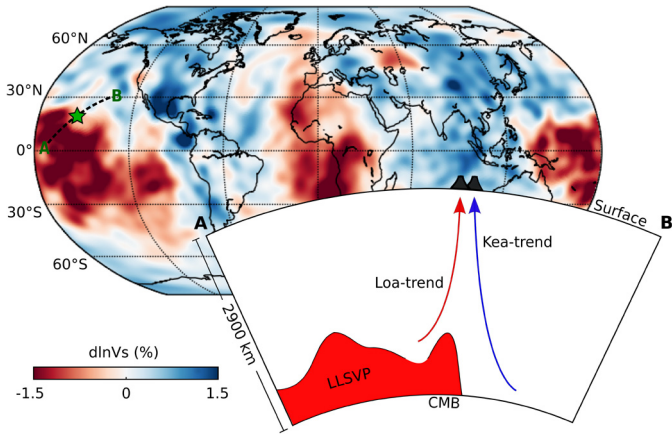
Fig. 1. The Hawaiian hotspot (green star), plotted above the shear-wave tomography model S40RTS (Ritsema et al., 2011) at 2800 km depth, illustrating that Hawaii overlies the boundary between a large region of low shear-wave velocities – the Pacific LLSVP – and surrounding mantle. Under the assumption that the Pacific LLSVP represents a chemically distinct body, Weis et al. (2011) hypothesise that geochemical differences between the Kea and Loa trends reflect preferential sampling of these two distinct sources of deep mantle material.

Huang et al., 2011; Farnetani et al., 2012; Hofmann and Farnetani, 2013; Payne et al., 2013; Harpp et al., 2014).

Weis et al. (2011) and Farnetani et al. (2012) hypothesise that the observed variations at Hawaii occur because the southern side of the Hawaiian plume preferentially samples less depleted material, from a distinct, large-scale geochemical reservoir in the deep-mantle: the Pacific large low shear-wave velocity province (LLSVP: see Fig. 1), a feature that is consistently imaged by seismological studies of the deep Pacific mantle (e.g. Houser et al., 2008; He and Wen, 2009; Ritsema et al., 2011). This hypothesis makes two central assumptions: (i) that the Pacific LLSVP represents a long-lived chemically distinct structure, termed a thermo-chemical pile (e.g. Tackley, 1998; McNamara and Zhong, 2005; Garnero and McNamara, 2008; Bower et al., 2013); and (ii) that source-region heterogeneities are transported into and preserved within a plume conduit (i.e. not stirred), as the plume rises from the deep-mantle to Earth's surface. Although the Pacific LLSVP's thermo-chemical structure is strongly debated (e.g. Garnero and McNamara, 2008; Simmons et al., 2009; Schuberth et al., 2009, 2012; Davies et al., 2012, 2015a), and it is unclear whether or not mantle plumes can preserve the heterogeneous structure of their boundary-layer source region during plume ascent, the interpretation of Weis et al. (2011) and Farnetani et al. (2012) has been extended to several other volcanic island chains in the Pacific, namely Marquesas, Samoa, Society, Galápagos and Easter (e.g. Huang et al., 2011; Payne et al., 2013; Harpp et al., 2014; Jackson et al., 2014). However, observations from the Samoan hotspot appear inconsistent with this hypothesis. Samoa lies on the southern margin of the Pacific LLSVP and, accordingly, the northern side of the Samoan plume would be expected to preferentially sample isotopically enriched material: the opposite trend is observed, with the Malu (southern) track exhibiting more enriched compositions, when compared to the Vai (northern) track (Huang et al., 2011).

There is no doubt that plumes carry a message from Earth's lowermost mantle. However, as illustrated by conflicting observations for Samoa and Hawaii, deciphering this message is challenging. The most systematic laboratory and computational studies undertaken, thus far, have focused on geochemical domains that are passive: that is, they lack any physical property contrast from surrounding mantle (e.g. Kerr and Mériaux, 2004; Farnetani and Hofmann, 2010; Farnetani et al., 2012). However, it has been recognised, in both numerical simulations and laboratory experiments, that the incorporation of active compositional heterogeneity

(i.e. heterogeneity that differs from ambient mantle in its material properties) strongly influences the dynamics of upwelling mantle plumes (e.g. Tackley, 1998; Jellinek and Manga, 2002; Farnetani and Samuel, 2005; Lin and van Keken, 2006a, 2006b; Davies et al., 2012; Steinberger and Torsvik, 2012).

In this study we use the computational modelling framework Fluidity (e.g. Davies et al., 2011; Kramer et al., 2012; Le Voci et al., 2014; Garel et al., 2014) to explore the parameter space over which the spatial distribution of geochemical domains in the lowermost mantle is preserved in plume conduits during plume ascent, in 2-D and 3-D. Specifically, we build on and complement earlier studies by, for example, Kerr and Mériaux (2004), Farnetani and Hofmann (2010) and Farnetani et al. (2012), and examine the effects of density and rheological variations between initially distinct and separate source components on plume stability, source entrainment and the stirring of these components. Included in our parameter search is the density and viscosity range predicted for LLSVPs as possible long-lived, thermo-chemical piles (e.g. Tackley, 1998; McNamara and Zhong, 2005; Deschamps and Tackley, 2008, 2009; Cobden et al., 2009). Our goal is to further test the hypothesis of Weis et al. (2011) and Farnetani et al. (2012) in the presence of chemical density and viscosity contrasts between different chemical domains.

2. Methods

We solve the Stokes and energy equations relevant to mantle convection using Fluidity, a finite-element, control-volume model with several state-of-the-art features (e.g. Davies et al., 2011; Kramer et al., 2012). We also solve for a volume fraction field that tracks the presence of a chemically distinct reservoir (Wilson, 2009). Fluidity: (i) uses an unstructured mesh, which enables the straightforward representation of complex geometries; (ii) dynamically optimizes this mesh, providing increased resolution in areas of dynamic importance, thus allowing for accurate simulations across a range of length-scales, within a single model; (iii) enhances mesh optimization using anisotropic elements; (iv) is optimized to run on parallel processors and has the ability to perform parallel mesh adaptivity; (v) utilises the highly-scalable parallel linear system solvers available in PETSc (Balay et al., 1997), that can handle sharp, orders of magnitude variations in viscosity; and (vi) has a novel interface-preservation scheme, which conserves material volume fractions, and allows for the incorporation of distinct chemical components (Wilson, 2009; Garel et al., 2014). In this study, Fluidity's adaptive mesh capabilities are utilised to provide a local resolution of 1 km in regions of dynamic significance (i.e. at the interface between materials and in regions of strong temperature, velocity and viscosity contrasts), with a coarser resolution of up to 100 km elsewhere.

Key model parameters are provided in Table 1. Simulations are undertaken in 2-D square and 3-D cubic domains of dimension 2900 km. Boundary conditions for temperature are $T = 273$ K at the surface, $T = 2073$ K at the base, with insulating (homogeneous Neumann) sidewalls. Velocity boundary conditions are free-slip and no normal flow at all boundaries. The material volume fraction, ϕ, is 1 inside the chemically distinct reservoir and 0 elsewhere. A 100-km thick stiff lithosphere is imposed at the top of the model, with a linear temperature profile between surface and underlying mantle. A temperature dependent viscosity is utilised, following the relation:

$$\eta(T^*) = \eta_0 \exp^{-bT^*} \qquad (1)$$

where $T^* = (T - T_{Surf})/(T_{CMB} - T_{Surf})$ is the non-dimensionalised mantle temperature. The reference viscosity, η_0, is multiplied by $\hat{\eta}_{lith}$ above 100 km depth and $\hat{\eta}_{660}$ below 660 km depth. Within

Table 1
Parameters common to all cases examined and their reference values.

Symbol	Parameter	Value	Units
α	Thermal expansion coefficient	3×10^{-5}	K^{-1}
η_0	Reference viscosity	5×10^{20}	Pa s
$\hat{\eta}_c$	Ratio of compositional to reference viscosity	0.1–10	–
$\hat{\eta}_{lith}$	Lithosphere viscosity multiplication factor	100	–
$\hat{\eta}_{660}$	660-km viscosity multiplication factor	30	–
ρ_0	Reference density	3300	$kg\,m^{-3}$
$\Delta \rho_c$	Contrast between compositional and reference density	0.0–100	$kg\,m^{-3}$
C_p	Specific heat capacity (at constant pressure)	1000	$J\,kg^{-1}\,K^{-1}$
D	Mantle depth	2900×10^3	m
g	Gravitational acceleration	9.8	$m\,s^{-2}$
κ	Thermal diffusivity	10^{-6}	$m^2\,s^{-1}$
T_{Surf}	Surface temperature	273	K
T_p	Background potential temperature	1573	K
T_{CMB}	CMB temperature	2073	K

Table 2
Distinct material properties of all cases examined. B = Buoyancy number; $\Delta \rho_c$ = chemical density contrast between the reservoir and background mantle; δ = parameter controlling the temperature dependence of viscosity; $\hat{\eta}_c$ = viscosity contrast between the reservoir and background mantle.

| B	$\Delta \rho_c$ (%)	δ	$\hat{\eta}_c$
0.0	0.0	0, 1, 2	0.1, 1, 10
0.025	0.0375	0, 1, 2	0.1, 1, 10
0.05	0.075	0, 1, 2	0.1, 1, 10
0.1	0.15	0, 1, 2	0.1, 1, 10
0.25	0.375	0, 1, 2	0.1, 1, 10
0.5	0.75	0, 1, 2	0.1, 1, 10
0.75	1.125	0, 1, 2	0.1, 1, 10
1.0	1.5	0, 1, 2	0.1, 1, 10
2.0	3.0	0, 1, 2	0.1, 1, 10

the chemically distinct reservoir η_0 is also multiplied by $\hat{\eta}_c$. The temperature dependence of viscosity is controlled by $b = \ln(10^\delta)$, where δ varies from 0 (isoviscous) to 2 (the maximum temperature induced viscosity contrast examined herein).

In our 2-D simulations a mantle plume is initiated in the lower thermal boundary layer (TBL) at the domain's centre via a Gaussian-shaped temperature perturbation, which is 200 km in height and 180 km between inflection points. The temperature is equal to T_p at the peak of the perturbation and increases linearly to T_{CMB} at the base of the model. A distinct geochemical reservoir ($\phi = 1$) is initialised in the domain's lower right hand corner with a Gaussian-shaped upper boundary. The reservoir material peaks at the domain's right hand boundary, at a height of 200 km, and has an inflection point 290 km left of the peak. In our 3-D simulations the plume is initialised at the centre of the domain within the lower TBL. We use a Gaussian-shaped temperature perturbation with the same dimensions as in the 2-D case, except that the distance between inflection points applies radially. The geochemical reservoir is initialised with the same planar dimensions as our 2-D case but is extended throughout the domain's entire 3-D extent.

We vary both the density contrast, $\Delta \rho_c$, and the viscosity contrast, $\hat{\eta}_c$, between the reservoir and background mantle, in addition to the temperature dependence of viscosity, to identify the parameter space over which the final conduit structure is indicative of the initial reservoir distribution. For each case, we specify a buoyancy number:

$$B = \frac{\Delta \rho_c}{\rho_0 \alpha \Delta T} \qquad (2)$$

which denotes the ratio of the (stabilising) chemical density contrast to the (destabilising) thermal density contrast ($\Delta T = T_{CMB} - T_p = 500$ K). All cases examined are summarised in Table 2. Our reference case ($B = \Delta \rho_c = 0.0$; $\hat{\eta}_c = 1$; $\delta = 2$) has a calculated
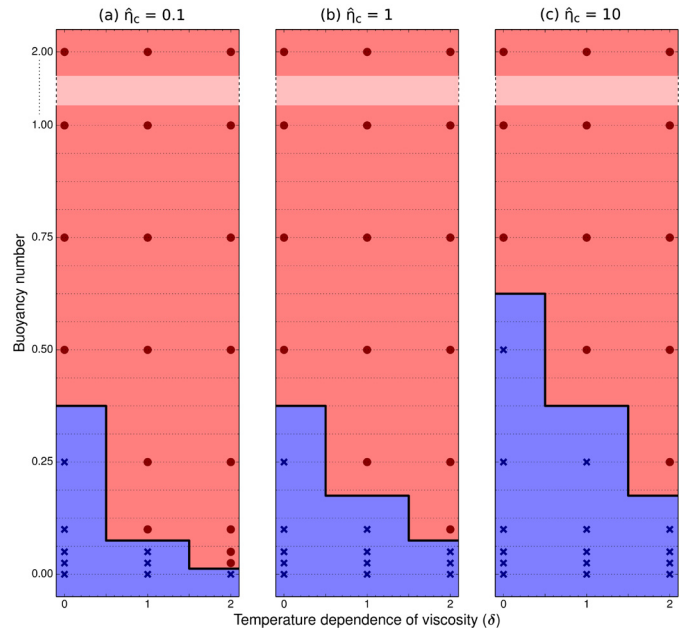
Fig. 2. Regime diagrams for conduit structure as a function of the Buoyancy Number, B, and the δ parameter controlling the temperature dependence of viscosity. Diagrams are presented for 3 different scenarios, where the viscosity contrast between the chemical reservoir and surrounding mantle, $\hat{\eta}_c$, is: (a) 0.1; (b) 1; and; (c) 10. Bilaterally asymmetric and concentric regimes are denoted by blue crosses and red circles, respectively.

buoyancy flux, Q, of $\approx 2.5 \times 10^4$ N/s, which is similar to the recent estimate for Hawaii (King and Adam, 2014).

3. Results and discussion

We first explore a wide parameter space (Table 2) in 2-D and find that two conduit regimes emerge: (i) a bilaterally asymmetric conduit structure; and (ii) a concentric conduit structure. The parameter space examined and the resulting conduit regimes are summarised in Fig. 2. The conduit regime is classified into bilaterally asymmetric or concentric via the ratio, R_c, of reservoir material on the left hand side of the conduit (i.e. the opposite side to which it entered) to the total amount of material on both sides of the conduit, at an upper mantle depth $d = 520$ km, as a function of time t,

$$R_c = \frac{\int_L \phi|_{z=D-d}\,ds}{\int_{L \cup R} \phi|_{z=D-d}\,ds} \qquad (3)$$

Here, ϕ is the reservoir volume fraction, s is the surface over which the integral is calculated, L is the conduit's left hand side, which

is separated from the conduit's right-hand-side, R, by the maximum conduit temperature. R_c is undefined until 1% of the total reservoir volume fraction has risen above height $z = D - d$. Once this condition is met, we classify the conduit structure as concentric if $R_c \geq 0.25$, and as bilaterally asymmetric if $R_c < 0.25$, for the simulation's entire duration.

To investigate how the two-dimensionality of our models influences results, we examine a subset of the parameter space in 3-D [$B = (0, 0.025, 0.05, 0.1, 0.25, 0.5)$, $\hat{\eta}_c = 1$, $\delta = 2$; and $B = 0.5$, $\hat{\eta}_c = (0.1, 10)$, $\delta = 2$]. We find that the 3-D simulations exhibit the same two conduit regimes identified in 2-D. Moreover, the transition from bilaterally asymmetric to concentrically zoned conduit structures is consistent with our 2-D results.

3.1. 2-D simulations

Fig. 3 illustrates a 2-D case where the plume adopts a bilaterally asymmetric structure. In such cases, a plume head forms above the thermal boundary layer and rises through the lower mantle with a trailing feeder conduit (Fig. 3a/b). As the plume enters the lower viscosity upper mantle, the head is stretched vertically, whilst the conduit thins. The plume subsequently impinges on the base of the lithosphere, spreading laterally (Fig. 3c). In this regime, the chemical reservoir migrates towards the foot of the plume, principally along the domain's base, where viscosities are at their lowest (Fig. 3d). Upon interaction with the plume conduit, this material rises along the proximal side of the conduit only (Fig. 3e) and, subsequently, is transported to the surface without lateral stirring across the conduit (Fig. 3f). Such conduit structures are consistent with those observed in previous studies (e.g. Kerr and Mériaux, 2004; Farnetani and Hofmann, 2010; Farnetani et al., 2012). In such a scenario, the spatial distribution of geochemical domains in the lowermost mantle is preserved during plume ascent (Fig. 3f, inset). In other words, spatio-temporal geochemical variations recorded at the surface could be related to an internal zonation of the underlying plume conduit that directly reflects the distribution of larger-scale geochemical heterogeneities in the lowermost mantle (e.g. Weis et al., 2011; Farnetani et al., 2012). We note that if the reference viscosity of dense material is identical to, or less than, ambient material, such bilaterally asymmetric conduit structures only occur where $B \lesssim 0.25$ (i.e. where the chemical effect on buoyancy is negligible). Where the reference viscosity of dense material is greater than ambient material, bilaterally asymmetric structures develop when $B \lesssim 0.5$.

At larger buoyancy numbers, the predicted conduit structure transitions from bilaterally asymmetric to concentric, with Fig. 4 illustrating a concentrically structured case. In these cases, the inherent asymmetry of the system modifies the flow regime, such that the plume's base migrates along the thermal-boundary-layer, away from the reservoir (Fig. 4b). As it does so, the conduit tilts, a process that is further enhanced as the plume enters the upper mantle (Fig. 4c). As the plume rises, material from the chemically dense reservoir moves laterally towards the conduit, eventually overshooting the conduit's central axis (Fig. 4d). The dense component's lateral motion is subsequently retarded by flow into the conduit from the opposite direction and, consequently, it gradually collects at the foot of the plume. Eventually, this dense material thickens to such an extent that thin tendrils are entrained into the conduit, with entrainment occurring exclusively within the conduit's central (hottest) region (Fig. 4e). This dense material remains at the conduit's central axis throughout its ascent to the surface (Fig. 4f), thus producing a concentric conduit structure (Fig. 4f, inset). Upon interaction with the overlying lithosphere, dense material spreads laterally to both sides of the domain, which differs from the bilaterally asymmetric cases, where material spreads to

one side only (cf. Figs. 3f and 4f). Under this concentric scenario, the spatial distribution of geochemical domains in the lowermost mantle is not preserved during plume ascent. As a consequence, the distribution of large-scale geochemical heterogeneities in the lowermost mantle cannot be discerned from surface observations. We find that concentric conduit structures persist at the maximum buoyancy number examined in this study, $B = 2$, with entrainment rates reduced as B is increased.

3.2. 3-D simulations

Fig. 5 illustrates a 3-D simulation where the plume adopts a bilaterally asymmetric structure. As in the equivalent 2-D case, a plume head forms above the thermal boundary layer and rises through the mantle with a trailing feeder conduit (Fig. 5a/b). As it enters the lower viscosity upper mantle, the head stretches and thins, and eventually impinges on the base of the lithosphere and spreads radially (Fig. 5c). In 3-D, the chemical reservoir is advected toward the inner conduit, along a radial path. As a result, material from the nearest part of the reservoir is the first to reach the conduit (Fig. 5b). This material rises up on the proximal side of the conduit only (Fig. 5c) and, upon interaction with the base of the lithosphere, spreads only to one side of the conduit and fans out (Fig. 6a). This process continues as more and more reservoir material is advected into the conduit's base. The result is a bilaterally asymmetric plume conduit, which is consistent with our equivalent 2-D case (Fig. 3) and with the predictions of previous studies (e.g. Kerr and Mériaux, 2004; Farnetani and Hofmann, 2010; Farnetani et al., 2012).

Despite differences in material advection into a plume conduit between 2-D and 3-D cases, the effect of varying $\Delta \rho_c$ remains the same: with increasing $\Delta \rho_c$, reservoir material migrates towards the conduit's base and eventually overshoots its central axis. Over time, this dense material thickens and is eventually entrained into the plume conduit, through its centre. Upon interaction with the base of the lithosphere, the dense material spreads radially in all directions (Fig. 6b) and, accordingly, any memory of the spatial distribution of deep-mantle domains is lost. In summary, our 2-D and 3-D results demonstrate that a small excess reservoir density can prevent deep-mantle structure from being preserved during plume ascent.

3.3. Key controlling parameters

The controlling role of the buoyancy number on the evolution of a chemically dense reservoirs has been recognised in previous studies (e.g. van Keken, 1997; Davaille, 1999; Oldham and Davies, 2004; Lin and van Keken, 2006a, 2006b; Deschamps and Tackley, 2009). Nonetheless, to illustrate how the effective (local) buoyancy number dictates material transport into mantle plumes, in Fig. 7, we plot its variation across the base of the plume conduit that is illustrated in Fig. 4. The temperature gradient across the conduit, from its hot central axis to its cool periphery, causes a decrease in the effective buoyancy number towards the conduit's central axis. In other words, the thermal effect on buoyancy is more dominant along the conduit centre and, hence, a plume can preferentially entrain dense material through its core, relative to its periphery. Accordingly, in the presence of significant density contrasts, the final distribution of chemical heterogeneities within a plume conduit will not be indicative of the heterogeneous nature of the plume's deep-mantle source region.

The temperature dependence of viscosity, and the relative viscosities of the different components, also play an important role. As the temperature dependence of viscosity is increased, concentric structures become more prevalent (Fig. 2), since dense material can flow through the lower thermal boundary layer and across
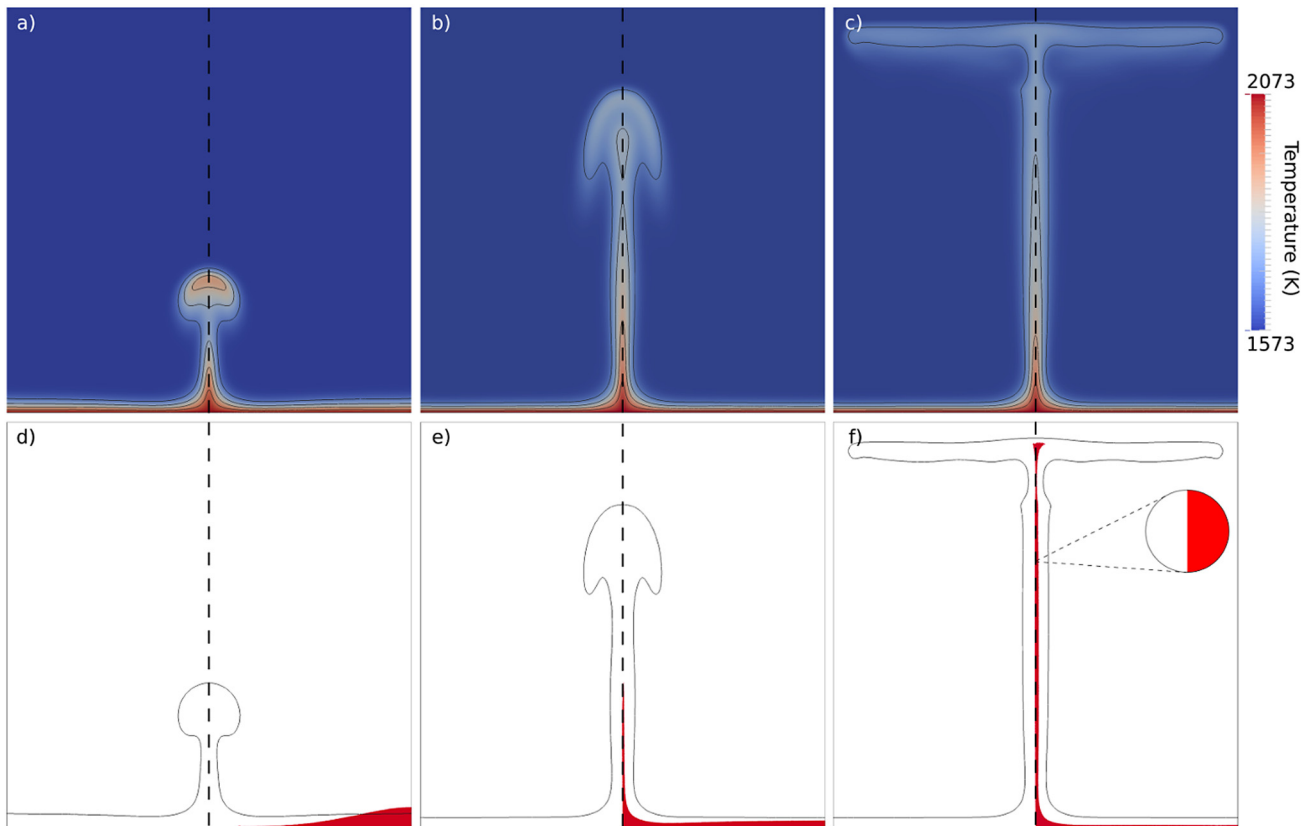
Fig. 3. (a)–(c) snapshots of the temperature field from a case where $B = \Delta \rho_c = 0.0$, $\hat{\eta}_c = 1$, and $\delta = 2$. The solid black line is the $T = 1660$ K temperature contour, whilst the dashed black line highlights the plume's central axis; (d)–(f) simultaneous snapshots of the compositional field (red), where $\phi = 0.5$, showing how a bilaterally asymmetric structure is preserved in the conduit as material ascends to the surface. Note that the inset shown in (f) represents a schematic cross-section of the inner conduit.
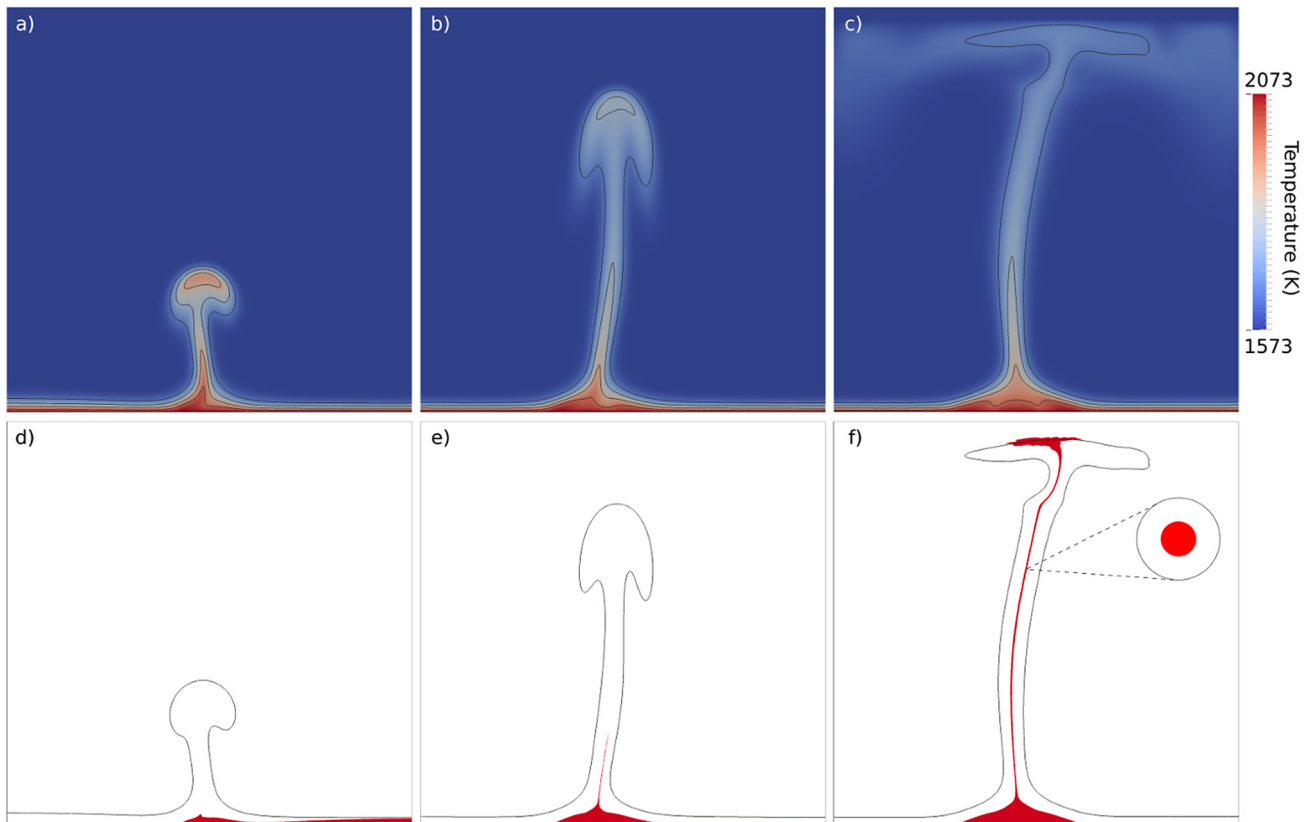
Fig. 4. As in Fig. 3, but for a case that adopts a concentric plume structure, where $B = 0.5$, $\Delta \rho_c = 0.75\%$, $\hat{\eta}_c = 1$, and $\delta = 2$. Under this scenario, the spatial distribution of geochemical domains in the lowermost mantle is not preserved during plume ascent.
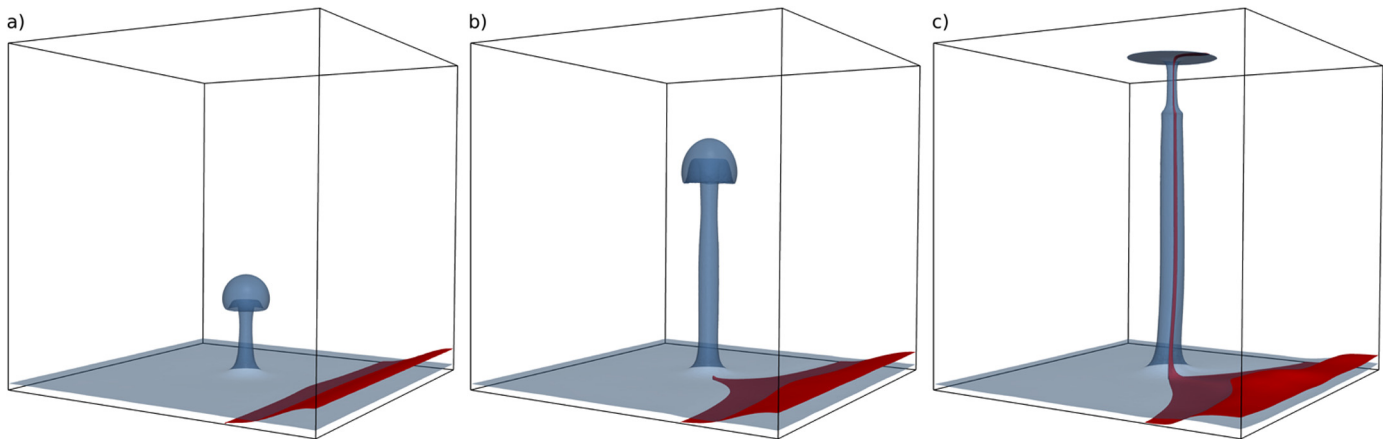
Fig. 5. (a)–(c) temporal snapshots of a 3-D simulation for a case where $B = \Delta\rho_c = 0.0$, $\hat{\eta}_c = 1$ and $\delta = 2$. The blue isosurface at $T = 1823$ K outlines the plume, whilst the red isosurface delineates the reservoir interface at $\phi = 0.5$, which illustrates how bilateral asymmetry develops within the conduit as the simulation evolves.
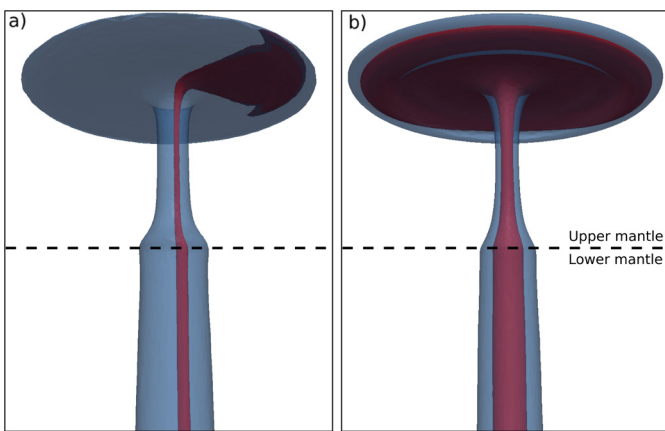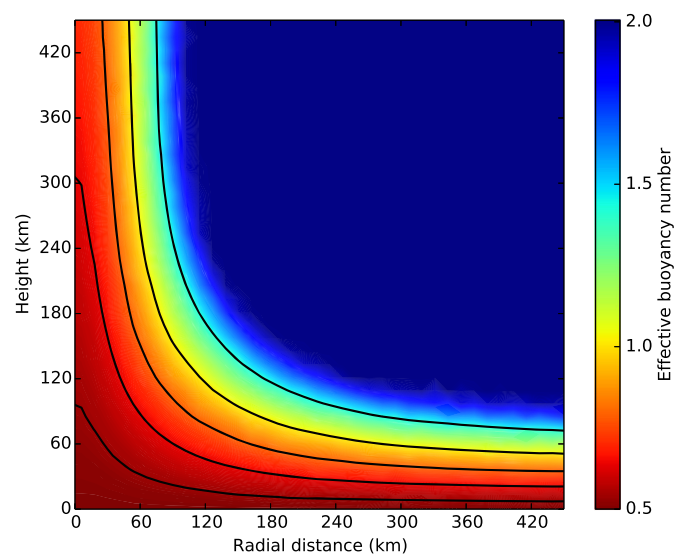

Fig. 6. Snapshots of the two dominant conduit regimes identified in this study. In both cases we plot a blue isosurface at $T = 1823$ K and the reservoir interface (red) at $\phi = 0.5$. The model parameters are: (a) bilaterally asymmetric: $B = \Delta\rho_c = 0.0$, $\hat{\eta}_c = 1$, and $\delta = 2$; and (b) concentric: $B = 0.5$, $\Delta\rho_c = 0.75\%$, $\hat{\eta}_c = 1$, and $\delta = 2$. The contrasting distribution of reservoir material beneath the lithosphere between the two regimes is apparent: only bilaterally asymmetric conduit structures can reliably map the location of the underlying mantle reservoir. For the concentric case, material beneath the lithosphere is dispersed radially and, thus, could have migrated into the conduit's base along any radial path.

Fig. 7. Plot of effective (local) buoyancy number across the base of the plume conduit illustrated in Fig. 4. Black lines are temperature contours at $T = 1750$, 1820, 1890, 1960 and 2040 K. The increased temperature at the conduit centre results in a corresponding decease in effective buoyancy number, illustrating why a plume can more readily sample dense material at its centre relative to its periphery. Note that this plot assumes that dense material, with $\Delta\rho_c = 0.75\%$, is present everywhere.

the conduit's central axis more easily. Decreasing (increasing) the dense reservoir's viscosity further enhances (discourages) this process and, hence, concentric structures become more (less) likely as $\hat{\eta}_c$ decreases (increases). Significantly, the trend towards concentric structures with increasing B and a greater temperature dependence of viscosity is maintained over a broad range of reservoir viscosities.

4. Implications and conclusions

Assigning the systematic patterns recorded in the geochemistry of hotspot lavas at Earth's surface to the heterogeneous structure and composition of Earth's deep-mantle is an attractive proposition (e.g. Weis et al., 2011; Huang et al., 2011; Farnetani et al., 2012). In this paper we have conducted a systematic 2-D and 3-D analysis of the conditions under which this is possible. Our models are intentionally simple, as our goal is to isolate the effects of chemical density and viscosity contrasts between different chemical domains.

Our results reveal that small variations in density between different chemical components will prevent the spatial distribution of geochemical domains in the lowermost mantle from being pre-

served during plume ascent. Given that oceanic crust and primitive iron-rich material, the most likely compositions to be sequestered in the lowermost mantle, are >2% denser than background mantle under deep-mantle conditions (e.g. Ringwood, 1975; Stixrude and Lithgow-Bertelloni, 2011), and similar or larger density contrasts are required to form stable, long-lived thermochemical piles (e.g. Tackley, 1998, 2002; McNamara and Zhong, 2004; Deschamps and Tackley, 2009; Davies et al., 2012), we conclude that it is premature to state that the heterogeneous structure and composition of Earth's lowermost mantle can be directly mapped from geochemical observations at Earth's surface (e.g. Weis et al., 2011; Farnetani et al., 2012). Indeed, if deep mantle LLSVPs are interpreted to be dense, stable and long-lived thermochemical piles, our results imply that the scenario proposed by Weis et al. (2011), Farnetani et al. (2012) and others (e.g. Huang et al., 2011; Payne et al., 2013; Harpp et al., 2014; Jackson et al., 2014), on the origin of the bilateral asymmetry recorded in Hawaiian and other Pacific hotspot lavas, is invalid: any memory of the spatial distribution of source-region heterogeneities will be lost during plume

ascent. The preservation of deep-mantle structure in hotspot lavas is further compounded by: (i) the orientation of a plume conduit relative to plate motion (e.g. Griffiths and Campbell, 1991; Farnetani and Hofmann, 2010; Harpp et al., 2014); and (ii) mixing in magma chambers, which has been shown to dominate the compositional evolution of basaltic melts on Iceland (e.g. Maclennan, 2008; Shorttle et al., 2014).

Alternatively, our results can be interpreted in another way. As noted previously, the thermo-chemical structure of deep-mantle LLSVPs is strongly debated (e.g. Garnero and McNamara, 2008; Deschamps and Tackley, 2008, 2009; Simmons et al., 2009; Schuberth et al., 2009, 2012; Davies et al., 2012, 2015a): several recent studies argue that their seismic characteristics can be explained by thermal heterogeneity alone, with chemical heterogeneity largely a passive component of lowermost mantle dynamics (i.e. its effect on density is outweighed by, or is secondary to, the effect of temperature) (see Davies et al., 2015a, for a detailed review). Under such a scenario, the hypothesis proposed by Weis et al. (2011), Farnetani et al. (2012) and others is more likely to hold. Indeed, not only would high-resolution geochemical observations from hotspot lavas at Earth's surface allow one to map the deep mantle's thermo-chemical structure, but they may also corroborate the thermally-dominant nature of lowermost mantle dynamics (Schuberth et al., 2009, 2012; Davies et al., 2012, 2015a). Further testing in global models that account for the effects examined herein, in addition to the complexities arising from subduction, background mantle flow and internal LLSVP structure, will be required to confirm this.

Our study has other important implications: Hofmann and White (1982) first proposed the hypothesis that plume related volcanism is derived from a source region that contains recycled oceanic crust. The success of this hypothesis in explaining the geochemistry of ocean island basalts (OIBs) has led to its widespread acceptance. The excess density of oceanic crust means that it should subduct and accumulate in the lowermost mantle, to dominate the primary source region of mantle plumes (e.g. Christensen and Hofmann, 1994; Davies, 2002; van Keken et al., 2002; Brandenburg and van Keken, 2007). We offer an additional argument as to why oceanic crust should be a prevalent component in OIBs: the excess density of oceanic crust, which causes it to subduct and sink to the base of the mantle, will also mean that it is preferentially sampled by the centre of plume conduits. Since the conduit centre is also the hottest part of the plume, it is: (i) the most likely part to melt; and (ii) likely to be the dominant source of picrites in plumes that undergo high degrees of partial melting.

Our conclusion that dense material in the lowermost mantle is preferentially sampled at the centre of plume conduits has further implications for how we interpret the geochemical evolution of Earth's deep-mantle. Campbell and Griffiths (1992) showed that recycled oceanic crust is absent from Archean plume magmas and does not make an appearance until ≈2.0 Ga, a conclusion supported by Blichert-Toft et al. (1996). If the basaltic component in mantle plumes is essential in explaining the geochemical signature of many OIBs (Hofmann and White, 1982) it must have been absent from the source of Archean mantle plumes: if present, it would have been preferentially sampled by the plume's central axis, which is most likely to melt and, thereby, enter the surface geological record. We therefore conclude that recycled basaltic crust did not enter the source region of mantle plumes, in significant volumes, until the Paleoproterozoic, perhaps reflecting the time taken for Earth's first oceanic lithosphere to sink to the core–mantle-boundary and return in plumes, as suggested by Campbell and Griffiths (1992).

References

Abouchami, W., Hofmann, A., Galer, S., Frey, F., Eisele, J., Feigenson, M., 2005. Lead isotopes reveal bilateral asymmetry and vertical continuity in the Hawaiian mantle plume. Nature 434, 851–856.

Allègre, C.J., Hofmann, A.W., O'Nions, R.K., 1996. The Argon constraints on mantle structure. Geophys. Res. Lett. 23, 3555–3557.

Balay, S., Gropp, W.D., McInnes, L.C., Smith, B.F., 1997. Efficient management of parallelism in object-oriented numerical software libraries. In: Modern Software Tools for Scientific Computing. Birkhäuser Boston Inc., pp. 163–202.

Ballmer, M.D., Ito, G., van Hunen, J., Tackley, P.J., 2011. Spatial and temporal variability in Hawaiian hotspot volcanism induced by small-scale convection. Nat. Geosci. 4, 457–460.

Ballmer, M.D., Ito, G., Wolfe, C.J., Solomon, S.C., 2013. Double layering of a thermochemical plume in the upper mantle beneath Hawaii. Earth Planet. Sci. Lett. 376, 155–164.

Ballmer, M.D., Ito, G., Cheng, C., 2015. Asymmetric dynamical behavior of thermochemical plumes and implications for Hawaiian lava composition. In: Hawaiian Volcanoes: From Source to Surface, pp. 35–57.

Bianco, T.A., Ito, G., van Hunen, J., Ballmer, M.D., Mahoney, J.J., 2008. Geochemical variation at the Hawaiian hot spot caused by upper mantle dynamics and melting of a heterogeneous plume. Geochem. Geophys. Geosyst. 9, Q11003.

Bianco, T.A., Ito, G., van Hunen, J., Ballmer, M.D., Mahoney, J.J., 2011. Geochemical variations at intraplate hot spots caused by variable melting of a veined mantle plume. Geochem. Geophys. Geosyst. 12, Q0AC13.

Blichert-Toft, J., Arndt, N., Ludden, J., 1996. Precambrian alkaline magmatism. Lithos 37, 97–111.

Bower, D.J., Gurnis, M., Seton, M., 2013. Lower mantle structure from paleogeographically constrained dynamic Earth models. Geochem. Geophys. Geosyst. 14, 44–63.

Brandenburg, J.P., van Keken, P.E., 2007. Deep storage of oceanic crust in a vigorously convecting mantle. J. Geophys. Res. 112, B06403.

Campbell, I.H., Griffiths, R.W., 1990. Implications of mantle plume structure for the evolution of flood basalts. Earth Planet. Sci. Lett. 99, 79–93.

Campbell, I., Griffiths, R., 1992. The changing nature of mantle hotspots through time: implications for the chemical evolution of the mantle. J. Geol. 100, 497–523.

Christensen, U.R., Hofmann, A.W., 1994. Segregation of subducted oceanic crust in the mantle. J. Geophys. Res. 99, 19867–19884.

Cobden, L., Goes, S., Ravenna, M., Styles, E., Cammarano, F., Gallagher, K., Connolly, J.A.D., 2009. Thermochemical interpretation of 1-D seismic data for the lower mantle: the significance of non-adiabatic thermal gradients and compositional heterogeneity. J. Geophys. Res. 114, B11309.

Davaille, A., 1999. Simultaneous generation of hotspots and superswells by convection in a heterogeneous planetary mantle. Nature 402, 756–760.

Davies, G.F., 1992. Temporal variation of the Hawaiian plume flux. Earth Planet. Sci. Lett. 113, 277–286.

Davies, G.F., 2002. Stirring geochemistry in mantle convection models with stiff plates and slabs. Geochim. Cosmochim. Acta 66, 3125–3142.

Davies, D.R., Davies, J.H., 2009. Thermally-driven mantle plumes reconcile multiple hot-spot observations. Earth Planet. Sci. Lett. 278, 50–54.

Davies, D.R., Wilson, C.R., Kramer, S.C., 2011. Fluidity: a fully unstructured anisotropic adaptive mesh computational modeling framework for geodynamics. Geochem. Geophys. Geosyst. 120, Q06001.

Davies, D.R., Goes, S., Davies, J.H., Schuberth, B.S.A., Bunge, H., Ritsema, J., 2012. Reconciling dynamic and seismic models of Earth's lower mantle: the dominant role of thermal heterogeneity. Earth Planet. Sci. Lett. 353, 253–269.

Davies, D.R., Goes, S., Lau, H.C.P., 2015a. Thermally dominated deep mantle LLSVPs: a review. In: Khan, A., Deschamps, F. (Eds.), The Earth's Heterogeneous Mantle. Springer International Publishing, pp. 441–477.

Davies, D.R., Goes, S., Sambridge, M., 2015b. On the relationship between volcanic hotspot locations, the reconstructed eruption sites of large igneous provinces and deep mantle seismic structure. Earth Planet. Sci. Lett. 411, 121–130.

Davies, D.R., Rawlinson, N., Iaffaldano, G., Campbell, I.H., 2015c. Lithospheric controls on magma composition along Earth's longest continental hotspot track. Nature 525, 511–514.

Deschamps, F., Tackley, P.J., 2008. Searching for models of thermo-chemical convection that explain probabilistic tomography: I. Principles and influence of rheological parameters. Phys. Earth Planet. Inter. 171, 357–373.

Deschamps, F., Tackley, P.J., 2009. Searching for models of thermo-chemical convection that explain probabilistic tomography: II. Influence of physical and compositional parameters. Phys. Earth Planet. Inter. 176, 1–18.

Dupré, B., Allègre, C.J., 1983. Pb–Sr isotope variation in Indian Ocean basalts and mixing phenomena. Nature 303, 142–146.

Farnetani, C.G., Hofmann, A.W., 2010. Dynamics and internal structure of the Hawaiian plume. Earth Planet. Sci. Lett. 295, 231–240.

Farnetani, C.G., Richards, M.A., 1994. Numerical investigations of the mantle plume initiation model for flood basalt events. J. Geophys. Res. 99, 13813–13833.

Farnetani, C.G., Richards, M.A., 1995. Thermal entrainment and melting in mantle plumes. Earth Planet. Sci. Lett. 136, 251–267.

Farnetani, C.G., Samuel, H., 2005. Beyond the thermal plume paradigm. Geophys. Res. Lett. 32, L07311.

Farnetani, C.G., Hofmann, A.W., Class, C., 2012. How double volcanic chains sample geochemical anomalies from the lowermost mantle. Earth Planet. Sci. Lett. 359–360, 240–247.

Garel, F., Goes, S., Davies, D.R., Davies, J.H., Kramer, S.C., Wilson, C.R., 2014. Interaction of subducted slabs with the mantle transition-zone: a regime diagram from 2-D thermo-mechanical models with a mobile trench and an overriding plate. Geochem. Geophys. Geosyst. 15, 1739–1765.

Garnero, E.J., McNamara, A.K., 2008. Structure and dynamics of Earth's lower mantle. Science 320, 626–628.

Griffiths, R., Campbell, I., 1991. On the dynamics of long-lived plume conduits in the convecting mantle. Earth Planet. Sci. Lett. 103, 214–227.

Harpp, K.S., Hall, P.S., Jackson, M.G., 2014. Galápagos and Easter: a tale of two hotspots. In: The Galapagos: A Natural Laboratory for the Earth Sciences, vol. 204, p. 27.

He, Y., Wen, L., 2009. Structural features and shear-velocity structure of the 'Pacific anomaly'. J. Geophys. Res. 114, B02309.

Hofmann, A.W., 2003. Sampling mantle heterogeneity through oceanic basalts: isotopes and trace elements. In: Treatise on Geochemistry. Elsevier, pp. 61–101.

Hofmann, A.W., Farnetani, C.G., 2013. Two views of Hawaiian plume structure. Geochem. Geophys. Geosyst. 14, 5308–5322.

Hofmann, A.W., White, W.M., 1982. Mantle plumes from ancient oceanic crust. Earth Planet. Sci. Lett. 57, 421–436.

Houser, C., Masters, G., Shearer, P., Laske, G., 2008. Shear and compressional velocity models of the mantle from cluster analysis of long-period waveforms. Geophys. J. Int. 174, 195–212.

Huang, S., Hall, P., Jackson, M.G., 2011. Geochemical zoning of volcanic chains associated with Pacific hotspots. Nat. Geosci. 4, 874–878.

Jackson, E.D., Shaw, H.R., Bargar, K.E., 1975. Calculated geochronology and stress field orientations along the Hawaiian chain. Earth Planet. Sci. Lett. 26, 145–155.

Jackson, M., Hart, S., Konter, J., Kurz, M., Blusztajn, J., Farley, K., 2014. Helium and lead isotopes reveal the geochemical geometry of the Samoan plume. Nature 514, 355–358.

Jellinek, A.M., Manga, M., 2002. The influence of a chemical boundary layer on the fixity, spacing and lifetime of mantle plumes. Nature 418, 760–763.

Kerr, R.C., Mériaux, C., 2004. Structure and dynamics of sheared mantle plumes. Geochem. Geophys. Geosyst. 5.

King, S.D., Adam, C., 2014. Hotspot swells revisited. Phys. Earth Planet. Inter. 235, 66–83.

Kramer, S.C., Wilson, C.R., Davies, D.R., 2012. An implicit free-surface algorithm for geodynamical simulations. Phys. Earth Planet. Inter. 194, 25–37.

Le Voci, G., Davies, D.R., Goes, S., Kramer, S.C., Wilson, C.R., 2014. A systematic 2-D investigation into the mantle wedge's transient flow regime and thermal structure: complexities arising from a hydrated rheology and thermal buoyancy. Geochem. Geophys. Geosyst. 15, 28–51.

Leitch, A.M., Davies, G.F., 2001. Mantle plumes and flood basalts: enhanced melting from plume ascent and an eclogite component. J. Geophys. Res. 106, 2047–2059.

Lin, S., van Keken, P.E., 2006a. Dynamics of thermochemical plumes: 1. Plume formation and entrainment of a dense layer. Geochem. Geophys. Geosyst. 7, Q02006.

Lin, S., van Keken, P.E., 2006b. Dynamics of thermochemical plumes: 2. Complexity of plume structures and its implications for mapping mantle plumes. Geochem. Geophys. Geosyst. 7, Q03003.

Maclennan, J., 2008. Concurrent mixing and cooling of melts under Iceland. J. Petrol. 49, 1931–1953.

McNamara, A.K., Zhong, S., 2004. Thermo-chemical structures within a spherical mantle. J. Geophys. Res. 109.

McNamara, A.K., Zhong, S., 2005. Thermo-chemical structures beneath Africa and the Pacific Ocean. Nature 437, 1136–1139.

Morgan, W.J., 1972. Deep mantle convection plumes and plate motions. Am. Assoc. Pet. Geol. Bull. 56, 203–213.

Oldham, D.N., Davies, J.H., 2004. Numerical investigation of layered convection in a three-dimensional shell with application to planetary mantles. Geochem. Geophys. Geosyst. 5, Q12C04.

Payne, J.A., Jackson, M.G., Hall, P.S., 2013. Parallel volcano trends and geochemical asymmetry of the Society Islands hotspot track. Geology 41, 19–22.

Richards, M.A., Duncan, R.A., Courtillot, V.E., 1989. Flood basalts and hotspot tracks: plume heads and tails. Science 246, 103–107.

Ringwood, A.E., 1975. Composition and Petrology of the Earth's Mantle. McGraw-Hill, New York.

Ritsema, J., van Heijst, H.J., Deuss, A., Woodhouse, J.H., 2011. S40RTS: a degree-40 shear velocity model for the mantle from new Rayleigh wave dispersion, teleseismic traveltimes, and normal-mode splitting function measurements. Geophys. J. Int. 184, 1223–1236.

Schuberth, B.S.A., Bunge, H.-P., Ritsema, J., 2009. Tomographic filtering of high-resolution mantle circulation models: can seismic heterogeneity be explained by temperature alone? Geochem. Geophys. Geosyst. 10, Q05W03.

Schuberth, B.S.A., Zaroli, C., Nolet, G., 2012. Synthetic seismograms for a synthetic Earth: long-period P- and S-wave traveltime variations can be explained by temperature alone. Geophys. J. Int. 200, 1393–1412.

Shorttle, O., Maclennan, J., Lambart, S., 2014. Quantifying lithological variability in the mantle. Earth Planet. Sci. Lett. 395, 24–40.

Simmons, N.A., Forte, A.M., Grand, S.P., 2009. Joint seismic, geodynamic and mineral physical constraints on three-dimensional mantle heterogeneity: implications for the relative importance of thermal versus compositional heterogeneity. Geophys. J. Int. 177, 1284–1304.

Steinberger, B., Torsvik, T.H., 2012. A geodynamic model of plumes from the margins of large low shear velocity provinces. Geochem. Geophys. Geosyst. 13, Q01W09.

Stixrude, L., Lithgow-Bertelloni, C., 2011. Thermodynamics of mantle minerals—II. Phase equilibria. Geophys. J. Int. 184, 1180–1213.

Tackley, P.J., 1998. Three-dimensional simulation of mantle convection with a thermo-chemical boundary layer: D"? In: Gurnis, M., Wysession, M.E., Knittle, E., Buffet, B.A. (Eds.), The Core–Mantle-Boundary Region. AGU, Washington, DC, pp. 231–253.

Tackley, P.J., 2002. Strong heterogeneity caused by deep mantle layering. Geochem. Geophys. Geosyst. 3, 1024.

Tatsumoto, M., 1978. Isotopic composition of lead in oceanic basalt and its implication to mantle evolution. Earth Planet. Sci. Lett. 38, 63–87.

van Keken, P., 1997. Evolution of starting mantle plumes: a comparison between numerical and laboratory models. Earth Planet. Sci. Lett. 148, 1–11.

van Keken, P.E., Hauri, E., Ballentine, C.J., 2002. Mantle mixing: the generation, preservation and destruction of chemical heterogeneity. Annu. Rev. Earth Planet. Sci. 30, 493–525.

Weis, D., Garcia, M.O., Rhodes, J.M., Jellinek, M., Scoates, J.S., 2011. Role of the deep mantle in generating the compositional asymmetry of the Hawaiian mantle plume. Nat. Geosci. 4, 831–838.

Wilson, C.R., 2009. Modelling multiple-material flows on adaptive unstructured meshes. Ph.D. Thesis. Imperial College London, UK.